Journal of Sound and Vibration 536 (2022) 117172

Contents lists available at ScienceDirect

Journal of Sound and Vibration

journal homepage: www.elsevier.com/locate/jsvi

Sound transmission through a panel with a hybrid active and semi-active control system

Stanislaw Wrona [a,*], Marek Pawelczyk [a], Li Cheng [b]

[a] Silesian University of Technology, Department of Measurements and Control Systems, Gliwice, Poland
[b] Department of Mechanical Engineering, Hong Kong Polytechnic University, Hong Kong, China

ARTICLE INFO

Keywords:
Hybrid control
Mathematical modelling
Acoustic radiation
Vibrating plates
Controllability
Control results

ABSTRACT

Semi-active control systems require significantly less energy than active solutions, while still providing substantial performance. However, active and semi-active systems can be applied in conjunction as hybrid systems, exploiting both solutions and providing high performance and reduced energy consumption. This paper proposes the use of such a hybrid active/semi-active control system for noise reduction barriers. Accounting for time-varying narrow-band noise, active structural acoustic control (ASAC) guarantees enhanced transmission loss for a noise barrier. Simultaneously, a semi-active element with a tunable mass moment of inertia allows the system to adapt to noise with varying characteristics by altering the mechanical properties of the barrier. Obtained control results demonstrate that the addition of a semi-active element is more effective than an additional active control actuator for reducing sound power in targeted frequency bands. Moreover, the proposed hybrid system may operate in two modes, allowing to further reduce overall energy consumption.

1. Introduction

Many applications use thin panels and shells as noise barriers to reduce the propagation of acoustic noise [1–6]. Even whole casings can be used in such a manner, what is detailed in [7]. Semi-active control systems can enhance the performance of aforementioned noise barriers. This can be accomplished either by the introduction of additional damping into the system using, for example, piezoelectric transducers and shunt circuits [8], or by shaping the frequency response of the barrier in order to adapt it to the current noise spectrum [9,10]. In both cases semi-active control systems are an attractive approach, because they require significantly less energy than the corresponding active solutions, while providing substantial performance [11]. Extending this, active and semi-active systems can be applied in conjunction as hybrid systems, exploiting both solutions and providing high performance and reduced energy consumption. The concept behind hybrid systems is not new. Harari et al. [12] proposed a hybrid vibration control system for a beam, where two piezoelectric actuators were controlled using contrasting techniques: one with an active control algorithm and the other with semi-active control. The aim was to realize the performance of an active control system, but with reduced energy consumption. Hiramoto et al. [13] studied a hybrid active/semi-active control scheme for motion and vibration control of mechanical and structural systems. Fu et al. [14] designed a hybrid active/semi-active isolation system with a fuzzy switching controller, integrated into a single-device magnetorheological elastomer isolator and piezoelectric stack actuator. Hasheminejad and Jamalpoor [15] investigated the control of sound transmission through a smart hybrid double sandwich panel partition. The hybrid structure included spatially distributed piezoelectric and electrorheological fluid actuator layers.

* Corresponding author.
E-mail addresses: stanislaw.wrona@polsl.pl (S. Wrona), marek.pawelczyk@polsl.pl (M. Pawelczyk), li.cheng@polyu.edu.hk (L. Cheng).

https://doi.org/10.1016/j.jsv.2022.117172
Received 30 August 2021; Received in revised form 30 June 2022; Accepted 3 July 2022
Available online 5 July 2022

Nomenclature

a	panel length
$A(f, z_s)$	acoustic response of the panel
b	panel width
c	sound velocity in air
D	flexural rigidity of the panel
E	Young's modulus of the panel
f	frequency
h	panel thickness
I_{sx}, I_{sy}	moments of inertia of the ith element
J	cost function
k_b	uniform spring constant
k_e	acoustic wavenumber
$\mathbf{K}$	total stiffness matrix
$\mathbf{K}_b, \mathbf{K}_p$	stiffness matrices corresponding to the strain energy of the boundary restraints and the panel, respectively
$m_{a,i}$	mass of the ith actuator
m_s	mass of the semi-active element
$\mathbf{M}$	total mass matrix
$\mathbf{M}_s, \mathbf{M}_a, \mathbf{M}_p$	mass matrices corresponding to the kinetic energy of the semi-active element, actuators, and panel, respectively
N	number of employed trial functions
N_a	number of actuators bonded to the panel's surface
$P_{ext,i}$	sound power corresponding to the ith vibration mode of the panel
$\mathbf{q}$	generalized panel displacement vector
$\mathbf{Q}$	vector of generalized forces
$\mathbf{R}_i$	ith radiation matrix
r_{mn}	the distance between mth and nth element
S_p	surface of the panel
T, T_s, T_a, T_p	overall kinetic energy of the system and kinetic energies of the semi-active element, actuators, and panel, respectively
$\mathbf{u}$	control vector
U, U_b, U_p	overall potential energy of the system and potential energies of the boundary restraints and the panel, respectively
$\mathbf{v}$	modal displacement vector
$w(x, y, t)$	displacement of the panel in the z-direction at time $t > 0$ and position (x, y)
z_s	distance of the element centre of the mass to the panel mid-plane
i, j, k	positive integers
x, y, z	coordinates in the global Cartesian coordinate system
$x_{a,i}, y_{a,i}$	coordinates of the ith actuator
$\imath$	imaginary number satisfying equation $\imath^2 = -1$
ν	Poisson's ratio of the panel
$\xi_{d,i}$	damping coefficient corresponding to the ith mode of the panel
$\boldsymbol{\Xi}$	damping matrix
ρ_e, ρ	air density and mass density of the panel material, respectively
$\phi_i(x, y)$	ith time-invariant trial function
$\boldsymbol{\phi}$	vector containing a set of time-invariant trial functions $\phi_i(x, y)$
$\boldsymbol{\Phi}$	eigenvector matrix
$\psi_{i,m}$	the modal velocity at the mth element
$\boldsymbol{\Phi}_i$	ith eigenvector (ith column in the eigenvector matrix $\boldsymbol{\Phi}$)
ω_i, $\boldsymbol{\Omega}$	ith eigenfrequency and the eigenfrequencies matrix, respectively

This paper proposes a novel hybrid active/semi-active control system for noise reduction barriers. Although the goal is to achieve synergy between active and semi-active approaches, a different strategy to those of the above examples is adopted. Assuming time-varying narrow-band noise, the active structural acoustic control (ASAC) guarantees enhanced transmission loss

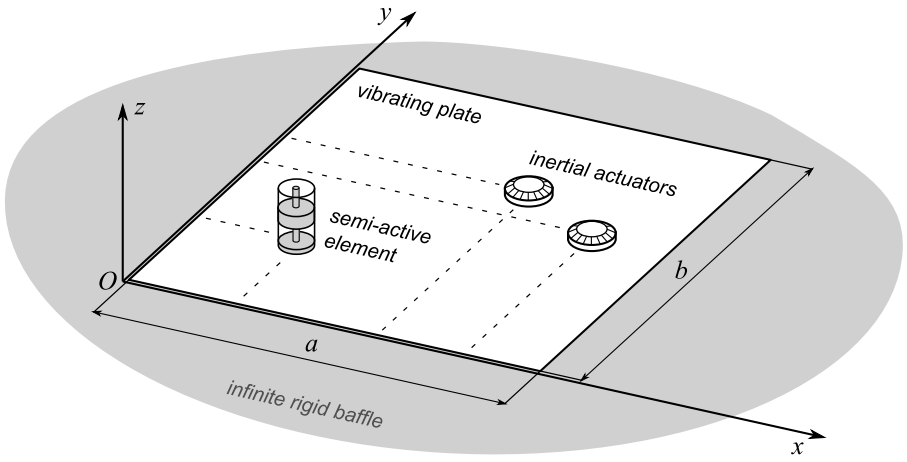

Fig. 1. A schematic representation of the vibrating plate with semi-active element and inertial actuators, situated within an infinite rigid baffle.

for a noise barrier. Simultaneously, a proposed semi-active element allows the system to adapt to noise with varying characteristics by altering the mechanical properties of the barrier. As an example of such semi-active component, an element with a tunable mass moment of inertia is used, which was previously employed by the authors to semi-actively shape the frequency response of a noise barrier [10]. In this paper, the semi-active element supports the active system, enhancing the controllability measures of the system at targeted frequency bands, thus increasing the level of noise reduction or reducing energy expenditure. That is, the semi-active part enhances the coupling between the actuators and the barrier, whereas the actuators are responsible for noise reduction. Although the controllability measures are not directly utilized in this paper (they are derived and used for example in [16]), the notion controllability is used to describe how energy-efficient is an active control of given modes.

When applied to individual barriers or entire device casings, ASAC systems demonstrate high performance [8,17]. To engender efficient operation of an active system, the actuators must be appropriately positioned [16]. Otherwise, the proximity of actuators to the nodal lines of particular mode shapes can make control of these modes infeasible. Thus, in order to control multiple modes in a wider frequency range, multiple actuators are required to find a balanced arrangement. The novelty of this paper lies in the combination of the semi-active element with the ASAC system.

The employed semi-active element consists of a mass mounted on a guide rod, which is attached perpendicularly to the surface of a panel (i.e., a noise barrier). The distance between the movable mass and the panel surface can be controlled, calibrating its effective mass moment of inertia. In this manner the semi-active element can modify the natural frequencies and mode shapes of the barrier during operation, thus adapting the mode shapes of the barrier's currently excited modes in order to facilitate their control via actuators. Such behaviour leads to either significantly enhanced noise reduction levels or reduced energy consumption of the system. The only energy required by the semi-active element is that used for shifting the movable mass; the mass can be held at a constant position without consuming energy.

It is important to note that this study and the proposed approach in general remains valid also for other semi-active devices capable of tuning the mechanical properties of the barrier. These may include any component that alters locally the stiffness or mass distribution of the panel, like ribs of tunable stiffness, concentrated masses that changes weight due to fluid flowing in or out, etc. An important common feature of these semi-active elements should be to require no energy to maintain a current state of the element. If so, the conclusions following from this study remains relevant for many different designs and structures that would be best fitted to particular application.

This paper is organized as follows. Section 2 introduces a mathematical model of the panel, the proposed semi-active element, and the actuators, including the impact of mass loading. Section 3 discusses the results of an experimental validation of the model. Section 4 presents and analyses numerical simulation studies based on the validated model and highlights the advantages conferred by the semi-active element. An energy-efficient hybrid control system, balanced between semi-active and active control parts is proposed. Section 5 summarizes the obtained results and concludes the paper.

2. Modelling the vibroacoustic system

This section models the vibroacoustic system, including the semi-active element and inertial actuators. For the sake of brevity, the description of model components already derived in [10] is limited to a minimum, however, the essentials are provided for reference. Fig. 1 shows a schematic representation of the system. The basis of the model is formed by a derivation of the free vibrations of an isotropic, rectangular plate with additional masses bonded to its surface. This requires the use of the Kirchhoff–Love theory of thin plates [18]. The Rayleigh–Ritz method is used to define an approximate solution to the eigenvalue equation, giving the natural frequencies and mode shapes of the vibrating system [19]. Finally, radiation mode theory is used to estimate the acoustic radiation generated by the obtained modes and the linear quadratic optimal control theory is used to evaluate the active control performance.

2.1. Modelling the panel vibration with actuators and semi-active elements

For an isotropic and homogeneous panel in the x–y plane, in a stress-free reference state, considering only the transverse motion and neglecting the effect of rotary inertia, the kinetic and strain energies of the panel, respectively T_p and U_p, can be written as

$$T_p = \frac{\rho h}{2} \iint_{S_p} \dot{w}^2 \mathrm{d}x\, \mathrm{d}y\,, \tag{1a}$$

$$U_p = \frac{D}{2} \iint_{S_p} \left\{ \left(\frac{\partial^2 w}{\partial x^2} \right)^2 + \left(\frac{\partial^2 w}{\partial y^2} \right)^2 + 2\nu \frac{\partial^2 w}{\partial x^2} \frac{\partial^2 w}{\partial y^2} + 2(1-\nu) \left(\frac{\partial^2 w}{\partial x \partial y} \right)^2 \right\} \mathrm{d}x\, \mathrm{d}y\,, \tag{1b}$$

where the integration region S_p corresponds to the surface of the panel, h is the panel thickness, $D = Eh^3/[12(1-\nu^2)]$ is the flexural rigidity of the panel, E is the Young's modulus of the panel, ν is the Poisson's ratio of the panel, ρ is the mass density of the panel, and the function $w(x, y, t)$ represents the displacement of the panel from the reference state in the z-direction at time $t > 0$ and position (x, y).

To allow for panels which are mounted imperfectly (i.e., neither simply-supported nor fully-clamped), the adopted boundary conditions are elastically restrained against rotation. The strain energy U_b stored in the rotational springs with spring constant k_b is given by:

$$U_b = \frac{k_b}{2} \left[\int_0^b \left\{ \left(\frac{\partial w}{\partial x} \right)^2 \Big|_{x=0} + \left(\frac{\partial w}{\partial x} \right)^2 \Big|_{x=a} \right\} \mathrm{d}y + \int_0^a \left\{ \left(\frac{\partial w}{\partial y} \right)^2 \Big|_{y=0} + \left(\frac{\partial w}{\partial y} \right)^2 \Big|_{y=b} \right\} \mathrm{d}x \right]. \tag{2}$$

The panel is subjected to semi-active control via a single semi-active element attached to its surface (additional elements could be incorporated analogously). As the semi-active element is assumed to be significantly smaller than the panel, the element can be modelled as a point mass located at a given distance from the panel surface. Hence, the total energy introduced to the system by the semi-active element is given by its kinetic energy T_s, which can be expressed as

$$T_s = \left\{ \frac{m_s}{2} \dot{w}^2 + \frac{I_{sx}}{2} \frac{\partial \dot{w}}{\partial x}^2 + \frac{I_{sy}}{2} \frac{\partial \dot{w}}{\partial y}^2 \right\} \Big|_{\substack{x=x_s \\ y=y_s}}, \tag{3}$$

where m_s is the mass of the semi-active element, I_{sx} and I_{sy} are the moments of inertia of the element, and x_s and y_s are the coordinates of the element. Considering the element as a point mass, the moments of inertia are $I_{sx} = I_{sy} = m_s z_s^2$, where z_s is the distance from the element centre of mass to the panel mid-plane.

In addition to the semi-active element, the panel also incorporates active control, thus forming a hybrid system. To provide active control, inertial actuators are bonded to the surface of the plate [20]. The actuators are smaller than the plate, and can therefore be modelled as additional concentrated masses. Assuming perfect bonding, the total energy introduced to the system by the actuators is given by their total kinetic energy T_a, expressed as

$$T_a = \sum_{i=1}^{N_a} \frac{m_{a,i} \dot{w}^2}{2} \Big|_{\substack{x=x_{a,i} \\ y=y_{a,i}}}, \tag{4}$$

where N_a is the number of actuators bonded to the surface of the panel, $m_{a,i}$ is the mass of the ith actuator, and $x_{a,i}$ and $y_{a,i}$ are the coordinates of the ith actuator.

2.2. The Rayleigh–Ritz method and the harmonic solution of the vibrating structure equation

In this section the Rayleigh–Ritz method is applied to the differential system in order to obtain its natural frequencies and mode shapes [19]. The adopted approach is analogous to the one described in [10].

The total energy of the system can be expressed as a function of the generalized panel displacement vector $\mathbf{q}$, the mass matrix $\mathbf{M}$ of dimension $N \times N$, and the stiffness matrix $\mathbf{K}$ of dimension $N \times N$. From Eqs. (1), (2), (3), and (4), the total kinetic energy, T, and the total potential energy, U, can be written as

$$T = T_p + T_s + T_a = \frac{1}{2} \dot{\mathbf{q}}^{\mathrm{T}} \mathbf{M} \dot{\mathbf{q}}\,, \qquad U = U_p + U_b = \frac{1}{2} \mathbf{q}^{\mathrm{T}} \mathbf{K} \mathbf{q}\,. \tag{5}$$

The total mass matrix $\mathbf{M} = \mathbf{M}_p + \mathbf{M}_s + \mathbf{M}_a$ is given by the sum of the matrices corresponding to each of the system components, where $\mathbf{M}_p$, $\mathbf{M}_s$ and $\mathbf{M}_a$ are the mass matrices of the panel, the semi-active element and the actuators, respectively. The total stiffness matrix $\mathbf{K} = \mathbf{K}_p + \mathbf{K}_b$ is also given by the sum of the matrices corresponding to each of the system components, where $\mathbf{K}_p$ and $\mathbf{K}_b$ are the stiffness matrices corresponding to the panel and boundary restraints, respectively.

From the stiffness and mass matrices, and by using the second-order Lagrange equation, the equation of a vibrating structure can be expressed as

$$\mathbf{M}\ddot{\mathbf{q}} + \mathbf{K}\mathbf{q} = \mathbf{Q}\,, \tag{6}$$

where $\mathbf{Q}$, of dimension $N \times 1$, is the vector of generalized forces. For optimization purposes, the action of the inertial actuators can be simplified and treated as a force acting on a point. Therefore, the control vector $\mathbf{u}$, of dimension $N_a \times 1$, can be defined as

$\mathbf{u} = \left[f_1, f_2, \dots, f_{N_a}\right]^{\mathrm{T}}$, where f_i is the force generated by the ith actuator. The vector of generalized forces can then be expressed as

$$\mathbf{Q} = \left[\boldsymbol{\phi}\Big|_{\substack{x=x_{a,1}\\y=y_{a,1}}}, \boldsymbol{\phi}\Big|_{\substack{x=x_{a,2}\\y=y_{a,2}}}, \dots, \boldsymbol{\phi}\Big|_{\substack{x=x_{a,N_a}\\y=y_{a,N_a}}}\right]\mathbf{u}\,. \tag{7}$$

The harmonic solution to Eq. (6) gives an eigenvector matrix $\boldsymbol{\Phi}$ of dimension $N \times N$ and N eigenfrequencies ω_i. Replacing $\mathbf{q}$ with $\boldsymbol{\Phi}\mathbf{v}$, and multiplying Eq. (6) on the left by $\boldsymbol{\Phi}^{\mathrm{T}}$, gives

$$\boldsymbol{\Phi}^{\mathrm{T}}\mathbf{M}\boldsymbol{\Phi}\ddot{\mathbf{v}} + \boldsymbol{\Phi}^{\mathrm{T}}\mathbf{K}\boldsymbol{\Phi}\mathbf{v} = \boldsymbol{\Phi}^{\mathrm{T}}\mathbf{Q}\,, \tag{8}$$

where $\mathbf{v} = \left[v_1, v_2, \dots, v_N\right]^{\mathrm{T}}$ denotes the modal displacement vector of dimension $N \times 1$. By exploiting the orthonormality of the eigenvectors in $\boldsymbol{\Phi}$, the modal mass matrix becomes a unit matrix $\mathbf{I}_N$ of dimension $N \times N$. Correspondingly, the total stiffness matrix becomes a diagonal matrix $\boldsymbol{\Omega}$ of N eigenvalues ω_i^2 [21]. Together, this gives

$$\boldsymbol{\Phi}^{\mathrm{T}}\mathbf{M}\boldsymbol{\Phi} = \mathbf{I}_N\,, \tag{9a}$$

$$\boldsymbol{\Phi}^{\mathrm{T}}\mathbf{K}\boldsymbol{\Phi} = \boldsymbol{\Omega} = \left[\mathrm{diag}(\omega_1^2, \omega_2^2, \dots, \omega_N^2)\right]\,. \tag{9b}$$

Substituting Eq. (9) in Eq. (8) then gives

$$\ddot{\mathbf{v}} + \boldsymbol{\Omega}\mathbf{v} = \boldsymbol{\Phi}^{\mathrm{T}}\mathbf{Q}\,. \tag{10}$$

To better represent the behaviour of a real system, an additional term can be introduced to account for damping in the system:

$$\ddot{\mathbf{v}} + \boldsymbol{\Xi}\dot{\mathbf{v}} + \boldsymbol{\Omega}\mathbf{v} = \boldsymbol{\Phi}^{\mathrm{T}}\mathbf{Q}\,, \tag{11}$$

where $\boldsymbol{\Xi}$ is a diagonal matrix of dimension $N \times N$, defined as $\boldsymbol{\Xi} = \left[\mathrm{diag}(2\xi_{d,1}\omega_1, 2\xi_{d,2}\omega_2, \dots, 2\xi_{d,N}\omega_N)\right]$, where the damping ratios $0 < \xi_{d,i} < 1$ are calculated using the thermoelastic damping model for elastic plates described in [22].

2.3. Acoustic radiation

This subsection derives an estimate of the sound power radiated by the ith vibration mode of the panel. The adopted approach is based on radiation mode theory [8]. The panel is assumed to be situated within an infinite rigid baffle, as shown in Fig. 1. Considering that the panel is divided into N_P elements with equal area ΔS_p, then the sound power $P_{ext,i}$ can be approximated as a finite series

$$P_{ext,i} = \frac{\omega_i \rho_e}{4\pi} \sum_{m=0}^{N_P} \sum_{n=0}^{N_P} \psi_{i,m} \cdot \frac{\sin(k_e\, r_{mn})}{r_{mn}} \cdot \psi_{i,n}^{*}\, \Delta S_p\, \Delta S_p\,, \tag{12}$$

where $\psi_{i,m}$ and $\psi_{i,n}$ are the modal velocity at the mth and nth element, respectively; the modal velocity is obtained by $\psi_{i,m} = -\imath\,\omega_i \boldsymbol{\Phi}_i^{\mathrm{T}}\boldsymbol{\phi}\Big|_{x=x_m, y=y_m}$, where x_m and y_m are the coordinates of the mth element; r_{mn} is the distance between mth and nth element; ρ_e and c are the density of air and the speed of sound in air, respectively; $k_e = \omega_i/c$ is the acoustic wavenumber; $\imath$ is the imaginary number $\sqrt{-1}$; and the superscript $*$ denotes complex conjugation. Eq. (12) can be noted in matrix form as

$$P_{ext,i} = \boldsymbol{\psi}_i^{\mathrm{H}}\, \mathbf{R}_i\, \boldsymbol{\psi}_i\,, \tag{13}$$

where symbol $\boldsymbol{\psi}_i = [\psi_{i,1}, \psi_{i,2}, \dots, \psi_{i,N_P}]^{\mathrm{T}}$; $\mathbf{R}_i$ is the radiation matrix; superscript H denotes the complex conjugate transpose. The mnth element of matrix $\mathbf{R}_i$ can be noted as

$$R_{i,mn} = \frac{\omega_i \rho_e (\Delta S_p)^2}{4\pi} \cdot \frac{\sin(k_e\, r_{mn})}{r_{mn}}\,. \tag{14}$$

It is noteworthy that the radiation matrix $\mathbf{R}_i$ depends on the geometry of the plate, acoustic environment parameters and frequency, but it does not depend on panel vibrations. The optimization process, described in the following part of the paper, requires to evaluate acoustic radiation efficiency of thousands of configurations in order to find the optimal solution. Thus, it is greatly beneficial to store and reuse radiation matrices already calculated for different frequencies, because it speeds up the optimization process dozens of times compared to usual Green's function approach used previously in [10].

2.4. Active control of the structure

The approach adopted to evaluate the active control performance is based on the linear quadratic optimal control theory [23,24]. The objective is to minimize the sound power of the structure. By means of additive theory, the velocity vector can be written as [8]

$$\boldsymbol{\psi} = \boldsymbol{\psi}_{pri} + \boldsymbol{\psi}_c = \boldsymbol{\psi}_{pri} + \boldsymbol{\psi}_{c\_unit}\mathbf{u}\,, \tag{15}$$

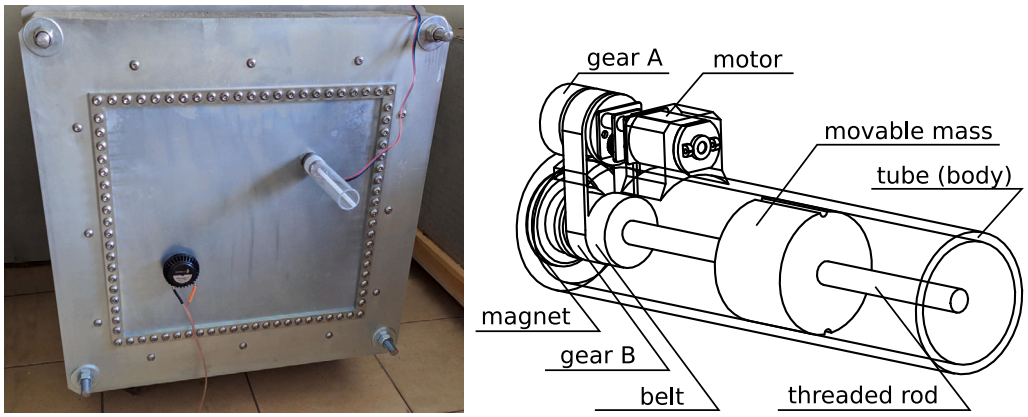

Fig. 2. The experimental setup. (a) A photograph showing the steel plate and heavy concrete box, along with an actuator and the semi-active element. (b) A schematic representation of the semi-active element.

where $\boldsymbol{\psi}_{pri}$ and $\boldsymbol{\psi}_{c\_unit}$ are the velocity due to the primary source and unit control source, respectively. Substituting Eq. (15) into Eq. (13), we obtain

$$P_{ext} = \mathbf{u}^{\mathrm{H}}\boldsymbol{\psi}^{\mathrm{H}}_{c\_unit}\mathbf{R}\boldsymbol{\psi}_{c\_unit}\mathbf{u} + \mathbf{u}^{\mathrm{H}}\boldsymbol{\psi}^{\mathrm{H}}_{c\_unit}\mathbf{R}\boldsymbol{\psi}_{pri} + (\boldsymbol{\psi}^{\mathrm{H}}_{c\_unit}\mathbf{R}\boldsymbol{\psi}_{pri})^{\mathrm{H}}\mathbf{u} + \boldsymbol{\psi}^{\mathrm{H}}_{pri}\mathbf{R}\boldsymbol{\psi}_{pri} \ . \tag{16}$$

Eq. (16) is a standard Hermitian quadratic form and it has a unique global minimum solution. Using linear quadratic optimal control theory, the solution can be expressed as

$$\mathbf{u}_{opt} = -[\boldsymbol{\psi}^{\mathrm{H}}_{c\_unit}\mathbf{R}\boldsymbol{\psi}_{c\_unit}]^{-1}[\boldsymbol{\psi}^{\mathrm{H}}_{c\_unit}\mathbf{R}\boldsymbol{\psi}_{pri}] \ . \tag{17}$$

It is noteworthy that the sound power is difficult to obtain in practice, however, the intention is to represent the maximum achievable noise reduction according to the actuators and semi-active element configuration.

2.5. Summary

The overall model derived in this section is a concise and coherent description of a vibroacoustic system that uses both active actuators and a semi-active element. The use of the Rayleigh–Ritz method facilitates the discovery of a numerical solution to the system. The radiation matrix approach greatly increases the computational efficiency. The linear quadratic optimal control theory is used to evaluate the active control performance. Together, these components comprehensively model the use of thin panels as hybrid active/semi-active noise barriers, as proposed by this paper. This model can be used to optimize the positioning of the actuators and semi-active elements and evaluate the efficiency of the obtained solution. As presented, the derivation represents a novel contribution of this paper.

3. Experimental setup and validation

This section describes the experimental validation of the model developed above. The experimental setup described here also constitutes the basis for the simulation studies presented in the following section.

The system consists of a rectangular steel plate mounted to a heavy concrete box and excited with a loudspeaker situated within the box. The loudspeaker is driven to generate a random, broadband noise (i.e., band-limited white noise). The concrete walls of the box provide a high degree of noise attenuation, and hence the majority of the acoustic energy that exits the box is transmitted through the steel plate. The acoustic excitation distribution across the plate is influenced to some extent by the acoustic modes of the box interior, however all of the vibration modes of the panel that can be theoretically expected in the considered frequency range were sufficiently excited to be detected by the laboratory equipment. A photograph of the experimental setup is shown in Fig. 2(a).

A schematic representation of the semi-active element is presented in Fig. 2(b). The element is attached to the plate surface using a neodymium magnet at its base. The chassis of the semi-active element, a hollow cylinder of poly-methyl methacrylate (PMMA), fits tightly around the movable mass within. The mass has a central threaded hole, by which it is mounted onto a threaded rod. The threaded rod is mounted on a ball-bearing at the base of the element, and can be rotated by a micro motor, via a belt transmission, thus controlling the distance z_s between the mass and the plate. The micro motor is equipped with an encoder which allows precise positioning of the mass.

The semi-active element can alter the natural frequencies and mode shapes of the plate by adjusting the distance z_s. This greatly influences the controllability of the system, which is highly relevant for active control. This phenomenon is caused by the change

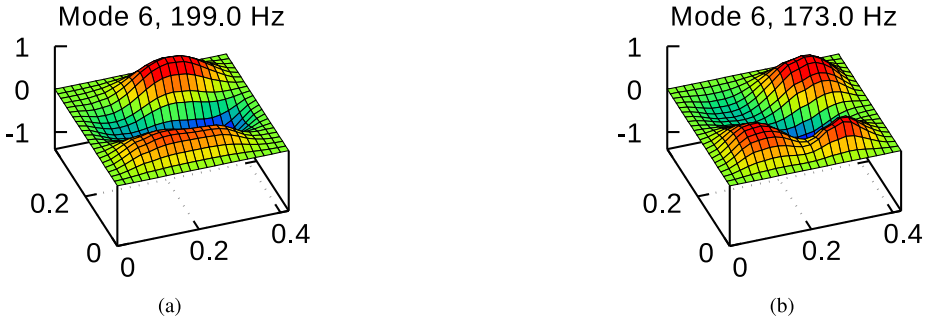

Fig. 3. A comparison of two mode shapes calculated with the mathematical model of the loaded panel, obtained with the semi-active element set for z_s = 0.01 m (a) and set for z_s = 0.04 m (b). The semi-active element was attached at x_s = 0.287 m, y_s = 0.098 m, with m_s = 0.081 kg. Size of the panel is in [m], and the z-axis depicts normalized amplitude.

Table 1
Parameters for the experimental setup.

Parameter	Value	Parameter	Value	Parameter	Value
a	0.420 m	ν	0.3	m_s	0.081 kg
b	0.390 m	k_b	340 N/rad	x_s	0.287 m
h	0.001 m	c	343 $^{m}/_{s}$	y_s	0.098 m
E	210 GPa	ρ_e	1.21 $^{kg}/_{m^3}$	z_s	0.05 m
ρ	7850 $^{kg}/_{m^3}$				

in modal mass of the modes, due to the altered mass moment of inertia of the semi-active element. However, in order for the mass moment of inertia of the element to affect a given mode, the element must "swing" while the mode vibrates. This is determined by the location of the semi-active element in relation to the particular mode shape: The rotations of the panel surface are highest at the nodal lines, and are absent at the anti-nodes, where the motion of the panel surface is solely translational. The increase in modal mass due to the semi-active element is local (not uniform). Hence, in addition to shifting the natural frequency of the mode, the mode shape is also altered in an irregular manner. This phenomenon has been depicted in Fig. 3, where 6th structural vibration mode was taken as an example. Fig. 3(a) shows a mode shape for z_s = 0.01 m, whereas Fig. 3(b) depicts altered mode shape of the same mode for z_s = 0.04 m. If a single actuator would be placed at $x_{a,1}$ = 0.10 m and $y_{a,1}$ = 0.16 m, the 6th mode would be nearly uncontrollable for z_s = 0.01 m (the actuator would be at a nodal line). However, by using the semi-active element and changing z_s to 0.04 m, the nodal line would be moved and the actuator would now be near an anti-node, making the considered mode perfectly controllable. Outside of controllability measures, this also affects the modal acoustic radiation efficiency.

Each inertial actuator used for the active control purpose is a commercially available Dayton Audio DAEX32EP-4. They are lightweight actuators (123 g) of small size (60 mm) relative to the plate. Each actuator is mounted to the plate magnetically, using neodymium magnets. The mathematical model accounts for the actuator mass, however due to their small height, the actuator moment of inertia is neglected. The inertial actuators, in contrast to semi-active elements, are most efficient at controlling modes when positioned at their anti-nodes (they generate force perpendicular to the panel surface). Hence, in order to improve the coupling between the actuators and the barrier for particular modes, the semi-active element alters the selected mode shapes in such a way that shifts their anti-nodes into the proximity of the actuators.

3.1. Experimental results

To validate the model, the panel with the semi-active element was used, adopting the parameters of the experimental setup as presented in Table 1 (cf. Section 2 for symbol definitions).

The value of k_b was obtained by preliminary experiments as described in [25]. These experiments used an optimization algorithm to minimize discrepancies in the natural frequencies and mode shapes between the mathematical model and experimental results.

The structural response of the vibrating panel was measured using a Polytec PDV-100 laser vibrometer. The structural responses present the measured signal magnitude in the logarithmic scale without any additional normalization. The vibration amplitudes measured with the laser vibrometer were between 100 and 500 mm/s. The vibrometer was mounted on an automatic positioning system which was developed by the authors. The positioning system allowed the carriage containing the vibrometer to be moved precisely along both the horizontal and vertical axes. Vibration measurements of the plate were taken over a total of 440 points. These points were arranged in a uniform grid of 22×20, spaced at intervals of 0.02 m, covering the entire surface of the plate. This spacing was sufficiently dense for measurement of the considered frequency range. Following measurement, the frequency at each point was analysed. The mode shapes were extracted by aggregating the estimated signal energy obtained for given frequencies of structural resonances (frequencies of consecutive modes) at all measurement locations.

To measure the acoustic response, two Beyerdynamic MM1 measurement microphones were mounted on the carriage with the laser vibrometer. The adopted dB reference is equal to one, i.e. the frequency responses present the measured signal magnitude in

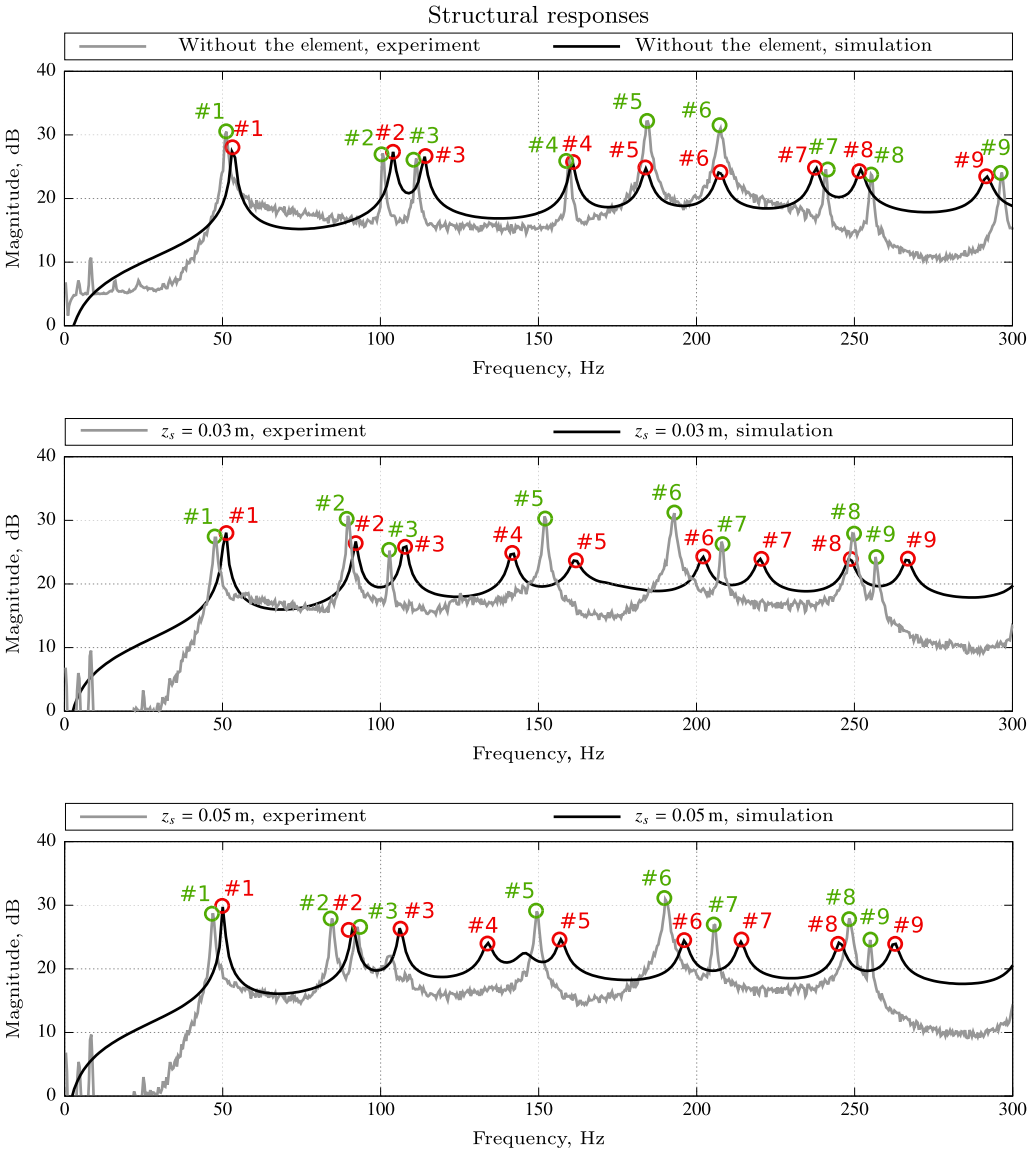

Fig. 4. Experimentally measured and simulated structural responses of the panel, obtained without (top) and with the semi-active element set for z_s = 0.03 m (middle), z_s = 0.05 m (bottom). The semi-active element was attached at x_s = 0.287 m, y_s = 0.098 m, with m_s = 0.081 kg. The coloured labels mark the corresponding mode numbers based on mode shapes analysis.

the logarithmic scale without any additional normalization. However, to give a feeling about the experiments, the Sound Pressure Level of the noise in the room was between 75 and 85 dB. The measurement procedure was analogous as for vibrations. A uniform measurement grid of 26×20 points was used, giving a total of 520 points, spaced at intervals of 0.04 m. The measurement grid was 1.00 m wide and 0.76 m high, and 0.1 m from the panel surface. The configuration of the laboratory setup corresponds more to near-field conditions (in contrast to far-field conditions adopted in the model). Therefore, additional acoustic radiation calculation method was used based on Green's function [16]. The acoustic response calculated with this approach averages sound pressure simulated at the measurement grid employed in experimental measurements. There are some minor differences when compared to acoustic responses obtained with radiation matrix method, but the consistency of both methods is very high.

The comparison of the experimental results with the theoretical predictions is given in Figs. 4–5. The top plots in both figures represents the unloaded panel, while the middle and bottom represent panel with the semi-active element. For the sake of brevity, plots for only two settings z_s = 0.03 m and z_s = 0.05 m are presented, however, the authors have carefully compared multiple configurations for all 10 settings of the semi-active element. The purpose of Figs. 4–5 is to show how the presence of the semi-active actuator affected the responses of the panel (both in experiment and simulation). For example: the first mode was slightly shifted towards lower frequencies; second and third modes were also shifted towards lower frequencies, and the second mode's

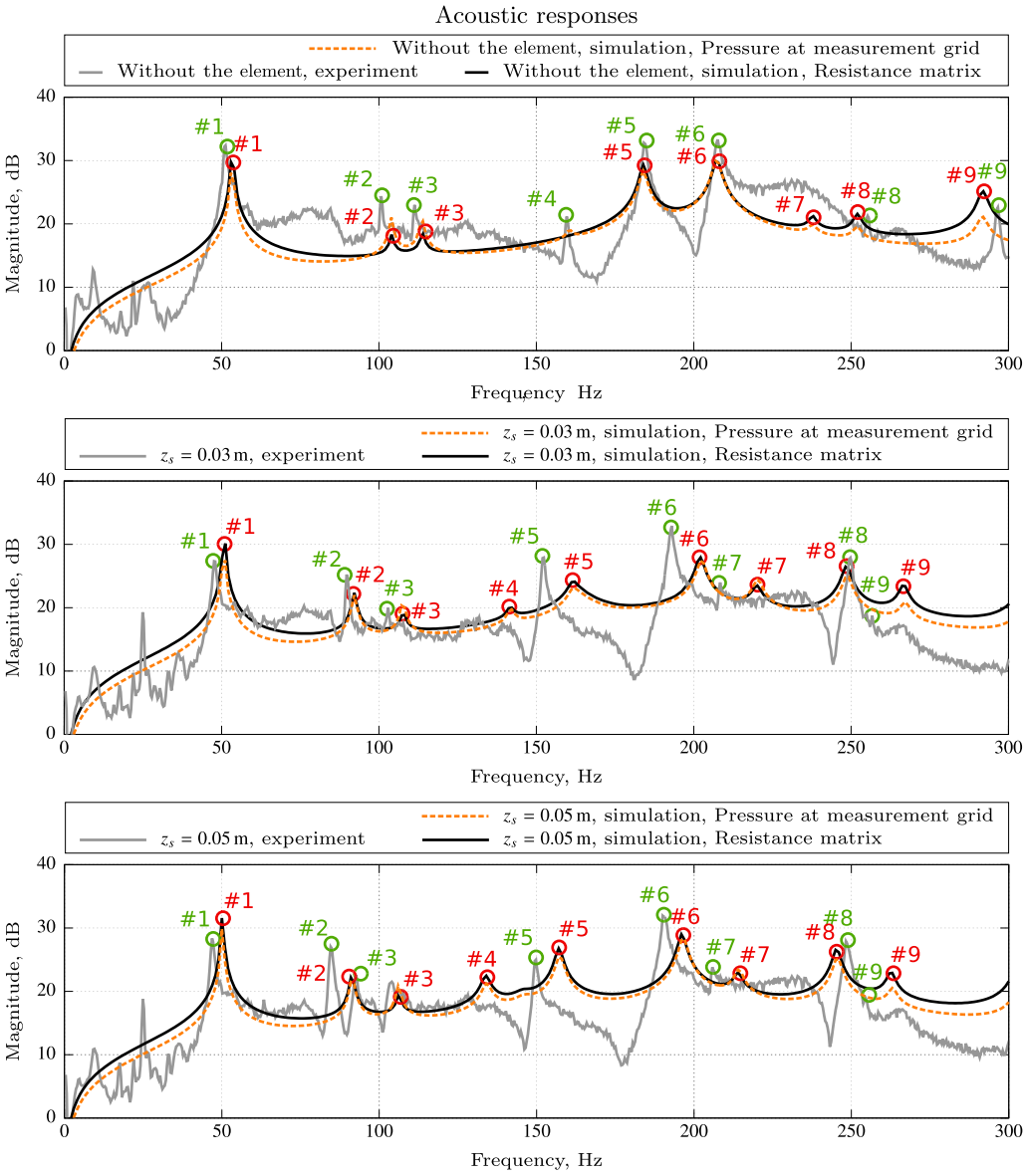

Fig. 5. Experimentally measured and simulated acoustic responses of the panel, obtained without (top) and with the semi-active element set for z_s = 0.03 m (middle), z_s = 0.05 m (bottom). The semi-active element was attached at x_s = 0.287 m, y_s = 0.098 m, with m_s = 0.081 kg. The coloured labels mark the corresponding mode numbers based on mode shapes analysis.

acoustic radiation was enhanced; the fourth mode is weakly noticeable in both cases; the fifth mode was strongly shifted left and its acoustic radiation was reduced; the sixth mode was also shifted left, but to a lesser extent, and its acoustic radiation was unaffected. Such analysis was done also for remaining modes and other configurations. On the other hand, comparing results for z_s = 0.03 m and z_s = 0.05 m, it is clear that increased distance z_s results in slight reduction of nearly all natural frequencies. The obtained experimental and simulated characteristics are coherent with respect to both the natural frequencies and estimated acoustic radiation, thus validating the model. The model is therefore suitable for use in the optimization problem and simulation studies presented in the following section. There are discrepancies between the model and the experiment, but it should be emphasized that during real application experimentally measured responses will be identified, stored, and used to determine the optimal setting of the semi-active element for current noise spectrum. Hence the imperfections of the model will be mitigated, as it is used to find more beneficial arrangement on the panel, but it is not used for the control purpose.

More details on the experimental setup, additional data and mode shapes visualizations can be found in [26], where the semi-active element was firstly introduced. On the other hand, the accuracy of modelling the actuators was also studied, e.g., in [16].

4. Simulation studies

Simulations were performed by adopting the panel parameters obtained in Section 3. Frequencies of up to 300 Hz were considered, corresponding with approximately the first ten eigenmodes of the panel. This section analyses and compares the acoustic responses of the panel in order to evaluate the noise reduction performance.

In all simulations, the excitation of the panel is generated by primary uniform excitation. It is induced by directly applying an equal excitation to all loaded structural modes, instead of explicitly simulating a specific acoustic or structural excitation. This approach is motivated by the requirement to design a barrier which can handle unknown excitations of potentially any mode (within a given frequency band). Therefore, during the optimization process, all modes should be considered in the simulated scenario to ensure that the actuators have sufficient control over them. This is an ideal scenario with which to evaluate the performance of the barrier for any kind of excitation, and provide a more general solution as the result of the optimization process.

The movable mass within the semi-active element is replaceable, allowing an appropriate mass to be fitted during the preparation phase. Hence, during the optimization process the total mass of the semi-active element (including the chassis) is also optimized, with a maximum value of 0.2 kg, corresponding to 15% of the panel's 1.3 kg mass. Considering potential practical applications and the advantages of simple solutions, a control system with minimal components is desirable. Hence, the simulation studies concern the optimization of a single semi-active element. This is sufficient to fulfil the requirements of the study, however additional elements can be incorporated to further enhance performance.

It can be assumed that the distance z_s is adjustable in the range from 0.01 m to 0.10 m, although in practice this range is a function of the overall setup, including the configuration of the semi-active element. For the purpose of optimization, the continuous domain of z_s is discretized with a step size of 0.01 m. Thus, 10 possible values of z_s are considered. The aim of the optimization process is to find the optimal positions of the semi-active element and actuators on the panel surface, considering all possible values of z_s. It is further assumed for the purpose of optimization that only a tonal noise will be attenuated by the barrier. Thus, during cost function evaluation, each frequency in the considered range (up to 300 Hz, in steps of 1 Hz) is evaluated individually with regards to choosing the most suitable value of z_s. Therefore, the finally presented response is aggregated basing on 10 responses for individual semi-active element's settings.

A population-based memetic algorithm was used to carry out the optimization. Each optimization process had a population consisting of 300 individuals (i.e., solutions); a maximum of 18 generations; and crossover, mutation, and individual learning probabilities of 0.20, 0.30, and 0.06, respectively. For a detailed introduction to memetic algorithms, see [27].

4.1. A single actuator

The panel considered in this study is intended for use as a hybrid active/semi-active noise barrier, which, when excited by either airborne sound or structural vibrations, should radiate as little noise to the environment as possible. To this end, the inertial actuators use ASAC to control the panel vibrations. Additionally, the semi-active element facilitates operation of the actuators by adapting properties of the panel to best handle the current noise spectrum. The semi-active element enhances the controllability measures of the system at targeted frequency bands, thus increasing the noise reduction level (if the control signal saturation was limiting the performance) or reducing energy expenditure (if highest possible performance due to other limitations was already reached).

The described objective is encapsulated by the cost function

$$J = \max_{f} \left[\min_{z_s} A(f, z_s) \right] , \tag{18}$$

where $A(f, z_s)$ is the acoustic response of the panel with active control turned on (calculated according to the Eq. (16)), as a function of both frequency f and distance z_s. Such a cost function enables the optimization algorithm to find a most efficient arrangement of actuators and the semi-active element, providing the highest possible acoustic insulation. In order to reflect practical system restrictions, a limit to the control signal amplitude $u_{max} = 0.3$ was adopted. The selection of u_{max} was arbitrary at this point, however, its impact on the optimization results is analysed in the following part of this Section.

Fig. 6a presents results for the use of a single actuator in a system without the semi-active element. The solution reached by the memetic algorithm positioned the actuator at $x_{a,1} = 0.312$ m and $y_{a,1} = 0.269$ m. The achieved levels of noise reduction do not exceed 5 dB due to the fact, that it is very difficult to find a location for a single actuator, which is balanced between multiple modes. As a result, only a minor reduction is achieved for all considered modes.

An improved configuration can be achieved with the addition of the semi-active element, as presented in Fig. 6b. The solution reached by the memetic algorithm positioned the actuator at $x_{a,1} = 0.124$ m and $y_{a,1} = 0.098$ m, and the semi-active element at $x_s = 0.184$ m and $y_s = 0.191$ m, with a mass of $m_s = 0.039$ kg. The levels of the noise reduction due to active control are approximately doubled when compared to the previous configuration without the semi-active element. It means that it is easier in terms of allowed control signal amplitudes (maximum energy expenditure) to control the modes by the actuator. Additionally, the response due to primary excitation is also significantly reduced. It means that the mode shapes were altered to reduce their acoustic radiation efficiency or that the modes can be beneficially shifted in the frequency domain in order to avoid their excitation by the primary narrowband noise. This effect was investigated in prior work, where frequency response shaping was considered using only the semi-active element [10]. Taking into account both of these phenomena, the acoustic barrier provides approximately 10 dB better noise reduction due to addition of the semi-active element. As already stated before, this conclusion is valid for a dominant

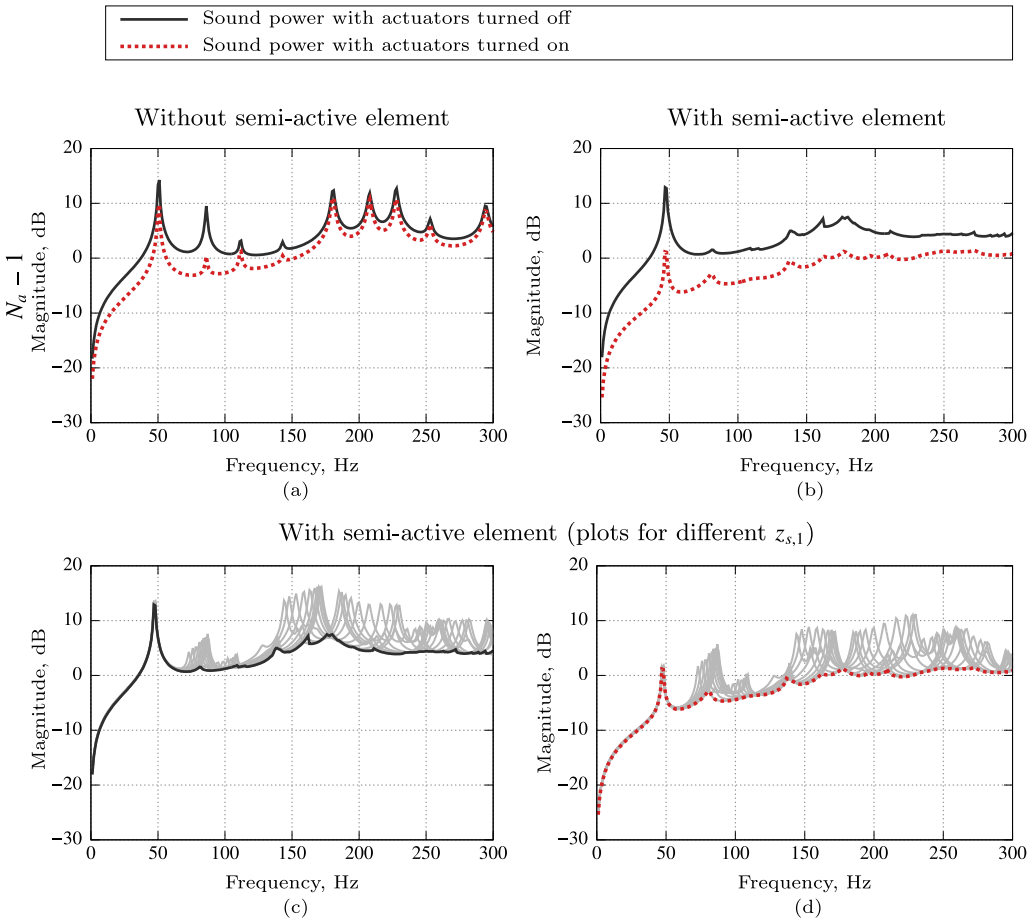

Fig. 6. Acoustic responses of the panel when using a single actuator ($N_a = 1$), both with and without the semi-active element. Sound power with the actuator turned off (black) and the actuator turned on (red) are shown. (a) Responses without use of the semi-active element. (b) Responses with the use of the semi-active element. (c)–(d) The indicated responses when using the optimal value of z_s, along with the corresponding variables when using all other possible values of z_s (grey). (For interpretation of the references to colour in this figure legend, the reader is referred to the web version of this article.)

single tone (or narrow-band) primary noise. The noise is allowed to be non-stationary, for example, due to changing the operating point of the devices generating the noise. Such devices are not uncommon in industry, as most rotating machinery (motors, shafts, fans, compressors, etc.) tend to generate dominant tonal noises, and also change their operating points, e.g., depending on different products on the assembly line; varying environmental/resources parameters; or after switching to another operating point made manually by the user or automatically after reaching certain states.

In case of broadband primary noise, the proposed approach would be much less efficient, however, even then its spectrum is very rarely flat, and then the proposed approach can be still beneficial if designed for the dominating subband.

To provide a better insight, Figs. 6c–d present each acoustic response together with the individual responses for each possible value of z_s. The optimal value of z_s for each frequency was derived by minimization of the function $A(f, z_s)$.

4.2. Multiple actuators

Fig. 7 presents results for the use of up to $N_a = 3$ actuators. It can be assessed that the active control part of the system performs well in all scenarios. It is mainly due to several facts: the noise is assumed to be periodical, what eliminates the potential issues of non-causality; the arrangement of actuators was optimized in all scenarios; the selected actuators' type (Dayton Audio DAEX32EP-4) transmission band covers all considered resonances, as they transmit vibrations well for frequencies higher than 40 Hz. As a result, the actuators' amplitude response was neglected in the model. Moreover, it is worth to note that such performance of active control system is entirely consistent with experimental results obtained by the authors for usual active structural acoustic control system, published e.g. in [28].

It can be observed that the addition of the semi-active element provides a greater improvement, both in terms of the cost function J and visual evaluation of frequency responses, than the addition of a further actuator. In addition to improved performance, control

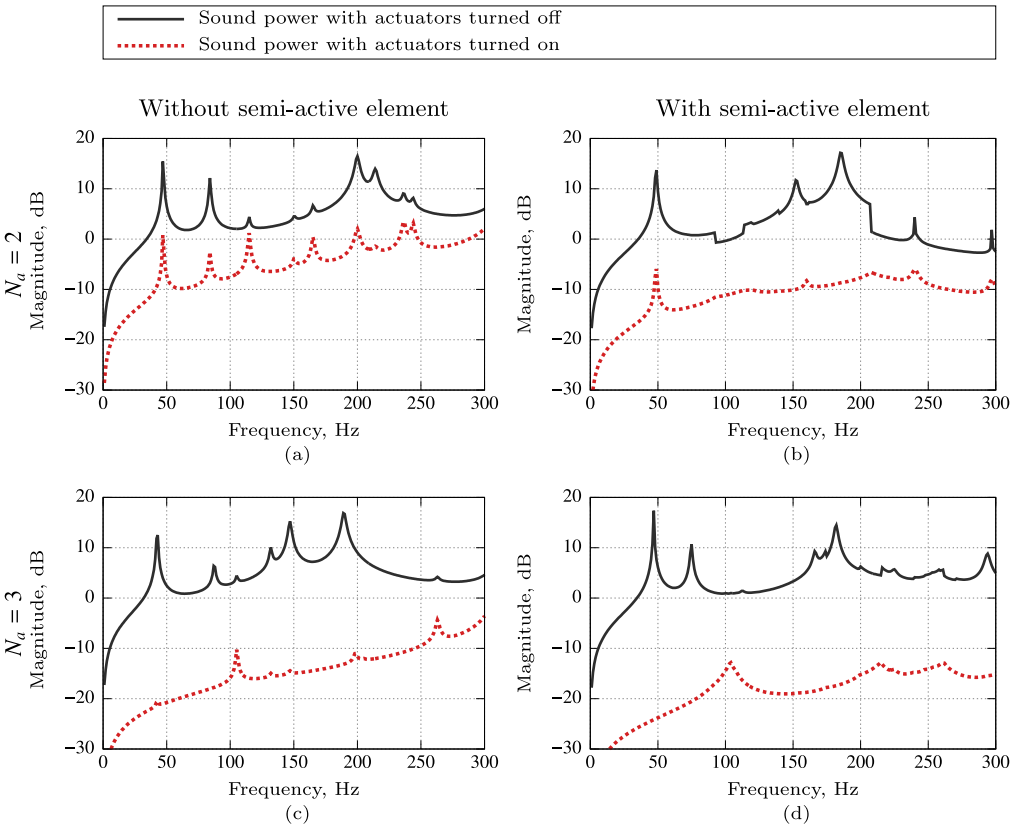

Fig. 7. Acoustic responses of the panel when using multiple actuators, both with and without the semi-active element. Sound power with actuators turned off (black) and actuators turned on (red) are shown. (a) $N_a = 2$, without the semi-active element. (b) $N_a = 2$, with the semi-active element. (c) $N_a = 3$, without the semi-active element. (d) $N_a = 3$, with the semi-active element. (For interpretation of the references to colour in this figure legend, the reader is referred to the web version of this article.)

Table 2
Optimized values of J, actuators position, semi-active element position and mass, for N_a equal to 1, 2 or 3.

		Without semi-active element						With semi-active element					
		N_a=1		N_a=2		N_a=3		N_a=1		N_a=2		N_a=3	
	J	**10.97 dB**		**3.35 dB**		**-3.58 dB**		**1.41 dB**		**-5.95 dB**		**-12.80 dB**	
Placement and mass	i	$x_{a,i}$ (m)	$y_{a,i}$ (m)	$x_{a,i}$ (m)	$y_{a,i}$ (m)	$x_{a,i}$ (m)	$y_{a,i}$ (m)	$x_{a,i}$ (m)	$y_{a,i}$ (m)	$x_{a,i}$ (m)	$y_{a,i}$ (m)	$x_{a,i}$ (m)	$y_{a,i}$ (m)
	1	0.312	0.269	0.112	0.179	0.329	0.090	0.124	0.098	0.049	0.194	0.333	0.142
	2			0.051	0.177	0.371	0.281			0.079	0.031	0.317	0.280
	3					0.191	0.215					0.090	0.061
								x_s (m)	y_s (m)	x_s (m)	y_s (m)	x_s (m)	y_s (m)
								0.184	0.191	0.228	0.198	0.197	0.170
								m_s (kg)		m_s (kg)		m_s (kg)	
								0.039		0.045		0.016	

of the semi-active element is more simple than that of an actuator. Moreover, the semi-active element consumes considerably less energy than an additional actuator, as the semi-active element only requires energy to switch state (i.e., to alter the distance z_s). The exact energy expenditure depends on particular signals in given scenario, however, less energy will be used with lesser number of actuators, making the whole system more energy-efficient, and therefore overall better.

Table 2 summarizes the optimization of each configuration using cost function J. The values of the cost function J, which reflect the overall noise reduction performance, confirm the above conclusions.

4.3. The balance between active and semi-active part of the system

In the numerical studies presented in this paper, the control signal limit was arbitrary chosen as $u_{max} = 0.3$. However, the adjustment of this parameter solely at the optimization phase, noted then u_{max}^{opt}, alters the found arrangement of actuators and the

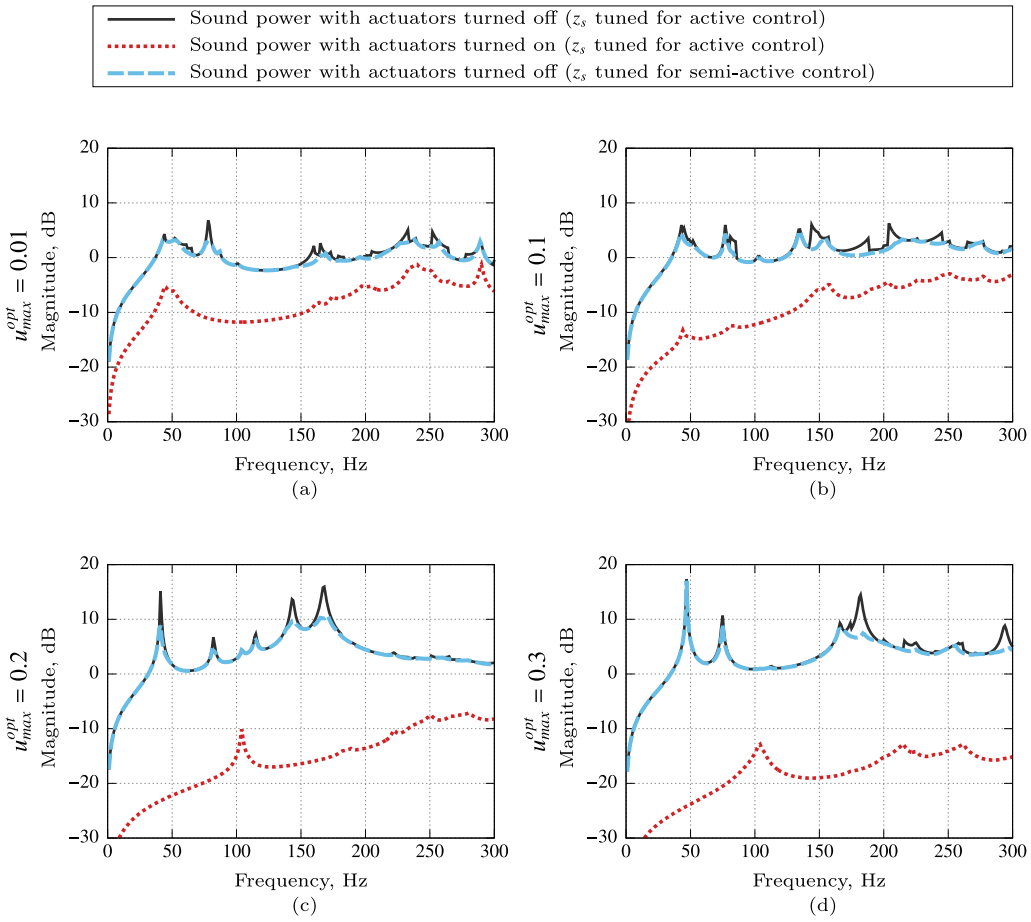

Fig. 8. Acoustic responses of the panel when using $N_a = 3$ actuators together with the semi-active element. Subfigures represent different values of u_{max}^{opt} used at the optimization step. (a) $u_{max}^{opt} = 0.01$. (b) $u_{max}^{opt} = 0.1$. (c) $u_{max}^{opt} = 0.2$. (d) $u_{max}^{opt} = 0.3$.

semi-active element. Namely, it is a way, among other options, to balance between the active and semi-active part of the control system. In the simulations calculated after the optimization step, actual $u_{max} = 0.3$ is always used for active control.

The greater the limit u_{max}^{opt} is adopted, the overall sound power can more rely on the active part of the system. Hence, the semi-active element role is focused to maximize the controllability measures, while the acoustic insulation due to barrier structure itself is less relevant. The sound power with the actuators turned off can be higher, assuming that it will be reduced due to active control effort.

In contrast, when the limit u_{max}^{opt} at the optimization stage is turned lower, the optimization algorithm seeks for more noise reduction due to semi-active element, apart from the actuators (the controllability measures are less important). Although the final noise reduction levels can be lowered due to such an approach, it would lead to more energy-saving solutions (the reduction will be provided more by semi-active part of the system). A representation of this phenomenon is shown in Fig. 8. In Fig. 8a, the parameter $u_{max}^{opt} = 0.01$, which means that optimization algorithm nearly neglect active control and tries to achieve noise reduction mainly through the semi-active element. It can be observed that the sound power magnitude without active control is on much lower levels compared to $u_{max}^{opt} = u_{max} = 0.3$ presented in Fig. 8d.

When u_{max}^{opt} is increased to 0.1, as presented in Fig. 8b, the sound power without active control is maintained at similar level, but the optimization algorithm takes now active control into account, hence actuators locations are more carefully selected, providing better levels of controllability. Thus, higher levels of noise reduction can be achieved when active control is turned on. Such configuration is well balanced for a hybrid control strategy, in which a noise barrier can operate in energy-saving mode when a user (recipient) is not in the direct proximity of the noise source; i.e. control system can employ solely the semi-active element, without actuators, providing approximately 10 dB of noise reduction when compared to a bare panel. However, if the presence of the user is detected and higher performance is required, then the actuators can be turned on and the semi-active element can be adjusted to support the active control. Such strategy may be more versatile and consume less energy in continuous operation.

5. Conclusions

This paper proposes a novel hybrid active/semi-active control system for noise reduction barriers. Active and semi-active systems are used in conjunction to provide both high performance and reduced energy consumption. Accounting for time-varying narrowband noise, ASAC guarantees enhanced transmission loss for a noise barrier. The proposed semi-active element, with a tunable mass moment of inertia, alters the mechanical properties of a barrier to adapt to noise with varying characteristics.

A mathematical model of the panel accounting for both inertial actuators and the proposed semi-active element has been derived and experimentally validated. Subsequently, numerical simulation studies based on the model were performed and analysed, demonstrating the advantages of using the semi-active element.

The results show that assuming a narrowband primary noise, the addition of the semi-active element provides a greater improvement in performance than the addition of a further actuator. In addition to improved performance, control of the semi-active element is more simple than that of an actuator. Moreover, the semi-active element consumes considerably less energy than an additional actuator, as the semi-active element only requires energy to switch state (i.e., to alter the distance z_s). Such behaviour either significantly enhances noise reduction or reduces energy consumption.

In addition, a balanced hybrid control system is proposed, which can operate in semi-active energy-saving mode without actuators, or in active/semi-active mode to provide full noise reduction performance.

It is important to emphasize, that the investigated hybrid approach and the drawn conclusions remains valid also for other semi-active devices capable of local alteration of stiffness or mass distribution of the panel. The particular design or structure depends on application requirements, however, the presented optimization approach and the technique for semi-active support of active control system remains valid.

This study shows that the use of a single semi-active element provides substantial benefits. However, the use of multiple semi-active elements would increase the dimensionality of the configuration space, thus further extending the capabilities of the proposed approach.

CRediT authorship contribution statement

Stanislaw Wrona: Conceptualization, Methodology, Software, Validation, Formal analysis, Investigation, Resources, Data curation, Writing – original draft, Writing – review & editing, Visualization. **Marek Pawelczyk:** Conceptualization, Validation, Writing – original draft, Writing – review & editing, Supervision, Project administration, Funding acquisition. **Li Cheng:** Conceptualization, Validation, Formal analysis, Writing – review & editing.

Declaration of competing interest

The authors declare that they have no known competing financial interests or personal relationships that could have appeared to influence the work reported in this paper.

Data availability

Data will be made available on request.

Acknowledgement

The research reported in this paper has been supported by the National Science Centre, Poland, decision no. DEC-2017/25/B/ST7/02236.

References

[1] K. Ege, M. Gallo, Q. Leclere, R.G. Rinaldi, N.B. Roozen, N. Totaro, Modeling, designing and measuring hybrid sandwich composite panels with optimized damping properties, in: Acoustic Black Holes and Structured Plates for Vibration Control, ABH2018, Le Mans, France, 2018.

[2] B. Lam, W.-S. Gan, D. Shi, M. Nishimura, S. Elliott, Ten questions concerning active noise control in the built environment, Build. Environ. 200 (2021) 107928.

[3] S. Wrona, M. Pawelczyk, Active reduction of device narrowband noise by controlling vibration of its casing based on structural sensors, in: Proceedings of 22nd International Congress on Sound and Vibration, Florence, Italy, 12-16 July, 2015.

[4] C.W. Isaac, M. Pawelczyk, S. Wrona, Comparative study of sound transmission losses of sandwich composite double panel walls, Appl. Sci. 10 (4) (2020) 1543, http://dx.doi.org/10.3390/app10041543.

[5] X.-X. Xie, Z.-X. Yuan, W.-B. Shangguan, Sound transmission loss of a metal panel with rib reinforcements and pasted damping, Int. J. Acoust. Vib. 25 (4) (2020) 513–525, http://dx.doi.org/10.20855/ijav.2020.25.41694.

[6] M. Misol, Full-scale experiments on the reduction of propeller-induced aircraft interior noise with active trim panels, Appl. Acoust. 159 (2020) 107086, http://dx.doi.org/10.1016/j.apacoust.2019.107086.

[7] M. Pawelczyk, S. Wrona, Noise-Controlling Casings, CRC Press, 2022, http://dx.doi.org/10.1201/9781003273806.

[8] Q. Mao, S. Pietrzko, Control of Noise and Structural Vibration, Springer, 2013.

[9] S. Wrona, M. Pawelczyk, L. Cheng, Semi-active links in double-panel noise barriers, Mech. Syst. Signal Process. 154 (2021) 107542, http://dx.doi.org/10.1016/j.ymssp.2020.107542.

[10] S. Wrona, M. Pawelczyk, L. Cheng, A novel semi-active actuator with tunable mass moment of inertia for noise control applications, J. Sound Vib. 509 (2021) 116244, http://dx.doi.org/10.1016/j.jsv.2021.116244.
[11] C.H. Hansen, Active Control of Noise and Vibration, CRC Press, 2013.
[12] S. Harari, C. Richard, L. Gaudiller, Hybrid active/semi-active modal control of smart structures, in: Active and Passive Smart Structures and Integrated Systems 2009, Vol. 7288, International Society for Optics and Photonics, 2009, p. 72881Z, http://dx.doi.org/10.1117/12.814094.
[13] K. Hiramoto, K.M. Grigoriadis, Active/semi-active hybrid control for motion and vibration control of mechanical and structural systems, J. Vib. Control 22 (11) (2016) 2704–2718.
[14] J. Fu, P. Li, G. Liao, J. Lai, M. Yu, Active/semi-active hybrid isolation system with fuzzy switching controller, J. Intell. Mater. Syst. Struct. 29 (1) (2018) 101–115, http://dx.doi.org/10.1177/1045389X17733054.
[15] S.M. Hasheminejad, A. Jamalpoor, Sound transmission control through a hybrid smart double sandwich plate structure, J. Sandw. Struct. Mater. (2020) 1099636220909764, http://dx.doi.org/10.1177/1099636220909764.
[16] S. Wrona, M. Pawelczyk, J. Cheer, Acoustic radiation-based optimization of the placement of actuators for active control of noise transmitted through plates, Mech. Syst. Signal Process. 147 (2021) 107009, http://dx.doi.org/10.1016/j.ymssp.2020.107009.
[17] K. Mazur, S. Wrona, M. Pawelczyk, Performance evaluation of active noise control for a real device casing, Appl. Sci. 10 (1) (2020) 337, http://dx.doi.org/10.3390/app10010377.
[18] S.S. Rao, Vibration of Continuous Systems, Vol. 464, Wiley Online Library, 2007.
[19] D. Young, Vibration of rectangular plates by the Ritz method, ASME J. Appl. Mech. 17 (4) (1950) 448–453.
[20] Q. Mao, S. Li, S. Huang, Inertial actuator with virtual mass for active vibration control, Int. J. Acoust. Vib. 25 (3) (2020) 445–452, http://dx.doi.org/10.20855/ijav.2020.25.31681.
[21] R.R. Craig, A.J. Kurdila, Fundamentals of Structural Dynamics, John Wiley & Sons, 2006.
[22] A.N. Norris, D.M. Photiadis, Thermoelastic relaxation in elastic structures, with applications to thin plates, Q. J. Mech. Appl. Math. 58 (1) (2005) 143–163, http://dx.doi.org/10.1093/qjmamj/hbi002.
[23] P.A. Nelson, S.J. Elliott, Active Control of Sound, Academic Press, 1991.
[24] C.C. Fuller, S. Elliott, P.A. Nelson, Active Control of Vibration, Academic Press, 1996.
[25] S. Wrona, M. Pawelczyk, Identification of elastic boundary conditions of light-weight device casing walls using experimental data, in: Proceedings of 21st International Conference on Methods and Models in Automation and Robotics, MMAR, IEEE, Międzyzdroje, Poland, 29 August - 1 September, 2016, http://dx.doi.org/10.1109/MMAR.2016.7575135.
[26] S. Wrona, M. Pawelczyk, X. Qiu, Shaping the acoustic radiation of a vibrating plate, J. Sound Vib. (2020) 115285, http://dx.doi.org/10.1016/j.jsv.2020.115285.
[27] F. Neri, C. Cotta, P. Moscato, Handbook of Memetic Algorithms, Vol. 379, Springer, 2012.
[28] S. Wrona, K. Mazur, J. Rzepecki, A. Chraponska, M. Pawelczyk, Reduction of compressor noise by the active casing approach, in: Proceedings of 26th International Congress on Sound and Vibration, Montreal, Canada, 7-11 July, 2019.